R744 Gas Cooler Model Development and Validation

J. M. Yin, C. W. Bullard and P. S. Hrnjak

ACRC CR-29 April 2000

For additional information:

Air Conditioning and Refrigeration Center
University of Illinois
Mechanical & Industrial Engineering Dept.
1206 West Green Street
Urbana, IL 61801

(217) 333-3115

The Air Conditioning and Refrigeration Center was founded in 1988 with a grant from the estate of Richard W. Kritzer, the founder of Peerless of America Inc. A State of Illinois Technology Challenge Grant helped build the laboratory facilities. The ACRC receives continuing support from the Richard W. Kritzer Endowment and the National Science Foundation. The following organizations have also become sponsors of the Center.

Amana Refrigeration, Inc.
Arçelik A. S.
Brazeway, Inc.
Carrier Corporation
Copeland Corporation
DaimlerChrysler Corporation
Delphi Harrison Thermal Systems
Frigidaire Company
General Electric Company
General Motors Corporation
Hill PHOENIX
Honeywell, Inc.
Hussmann Corporation
Hydro Aluminum Adrian, Inc.
Indiana Tube Corporation
Invensys Climate Controls
Lennox International, Inc.
Modine Manufacturing Co.
Parker Hannifin Corporation
Peerless of America, Inc.
The Trane Company
Thermo King Corporation
Visteon Automotive Systems
Whirlpool Corporation
Wolverine Tube, Inc.
York International, Inc.

For additional information:

Air Conditioning & Refrigeration Center
Mechanical & Industrial Engineering Dept.
University of Illinois
1206 West Green Street
Urbana IL 61801

217 333 3115

R744 Gas Cooler Model Development and Validation

Abstract

A first principles-based model was developed for a transcritical CO2 gas cooler, using a finite element method. The model uses published correlations for refrigerant and airside heat transfer and pressure drop. Experimental results are presented at 48 operating conditions. The model predicted the gas cooler capacity within ±2% and pressure drop on the R744 side well within the range of experimental error. The model's usefulness is demonstrated by analyzing alternative circuiting and multi-slab designs.

Introduction

Due to the global warming impact of HFC automobile air conditioning, much interest has been focused on the transcritical R744 cycle (Pettersen et al. 1994). This cycle has been well known for a long time and was revisited recently by Lorentzen and Pettersen (1993). The main difference between the R744 transcritical cycle and the conventional reversed-Rankine cycle is that the heat rejection process occurs at supercritical (>31° C) temperatures for most operating conditions. An internal heat exchanger is used downstream of the gas cooler to achieve a lower inlet quality to the evaporator and reduce the COP-maximizing operating pressure (Boewe, et al 1999a).

Recently the first detailed system performance comparisons were published by McEnaney et al. (1999) after Pettersen (1994). In an extensive set of experiments, a conventional off-the-shelf R134a system for a midsize car was compared to a prototype R744 system designed to have heat exchangers of the same volume and air side pressure drop. Results showed the R744 system to have slightly lower capacity and COP (few percent) at very high ambient temperatures (above 45°C) but much higher capacity and COP at lower ambient temperatures. The results also showed that when the ambient temperature is close to R744 critical temperature, the optimized high-side pressure is also reduced to a level close to R744 critical pressure, and the system COP has a sharp maximum value for a given operating condition. This behavior is due to the thermophysical property characteristics of R744 in the critical region. When the system operates at a higher ambient temperature, the COP vs pressure curve tends to become flatter.

The gas cooler is important to the performance of the transcritical CO2 air conditioning system for two reasons. First is the effect on system capacity which is maximized by rejecting heat to the surroundings instead of the internal heat exchanger. The system capacity can be maximized by reducing the refrigerant temperature at gas cooler exit to air inlet temperature. The internal heat exchanger also increases capacity, but at the cost of higher compressor work caused by suction gas heating. Therefore it is desirable to reject heat to the surroundings from the gas cooler. Second, improving gas cooler performance is very important because it reduces the COP-maximizing operating pressure, thus reducing compressor power.

The thermodynamic process in the gas cooler differs greatly from a condenser or ordinary gas-to-gas heat exchanger. The operating pressures range from subcritical to 140bar; and thermophysical properties vary strongly in the critical region, where specific heat approaches infinity. Cycle COP is very sensitive to the gas cooler outlet state. Many published

thermodynamic analysis were based on assumptions, rather than calculations, about the refrigerant temperature at the gas cooler exit (e.g. Robinson and Groll, 1998). In an actual cycle, this temperature changes with different operating conditions, and a good design can bring it closer to the ambient temperature.

This paper develops a model for analyzing the thermodynamic process in the gas cooler and studying the effect of thermophysical property variations on gas cooler performance. The simulations are then compared with a large and detailed set of experimental data.

Dimensions and characteristics of gas coolers

Figure 1 shows the gas cooler used in the experiments. It has three passes, consisting of 13, 11, and 10 tubes each. R744 flow enters the gas cooler through an inlet elbow, proceeds through three passes and exits through another exit elbow.

Figure 2 shows the cross-section of the microchannel tubes, and Table 1 gives the dimensions of the gas cooler itself.

Experimental data

The experiments were carried out in the mobile a/c system test facility described in detail by McEnaney (1998). The gas cooler was installed in a wind tunnel, which was located inside a calorimetric chamber. Pressure transducers were installed before the inlet elbow and after the exit elbow of the gas cooler. The temperatures of R744 at the gas cooler inlet and exit were measured by two immersed thermocouples. Refrigerant mass flow rate through the gas cooler was measured by using a Corolis type mass flow rate meter. The mass flow rate of air through the gas cooler was measured by a standard ASHRAE nozzle (Boewe, et al. 1999b). Inlet air temperature was measured by using a thermocouple grid, and air temperature after gas cooler was measured by using thermocouple mounted on the throat of the nozzle, which was located downstream of the mixer.

Data were recorded at 358 points clustered around 48 distinct indoor/outdoor operating conditions. The clusters resulted from systematically varying inlet pressure to find the optimal system COP. Table 2 shows one data point from each of 48 different operating conditions. The data range from 77 to 144bar for pressure, 27 to 55°C for air inlet temperature, 19 to 56g/s for the mass flow rate of supercritical CO2 and 450 to 710 g/s for air flow rate. The uncertainties for pressure, temperature and mass flow rate measurement were about 50kPa, 1°C and 0.1%, respectively. The resulting uncertainty for capacity measurement was about ±5%.

Simulation model

A finite element approach was used in the modeling of the gas cooler. As shown in Figure 3, each pass of the gas cooler is separated into 10 equal-length segments along the refrigerant flow direction. Each segment is treated as a cross-flow heat exchanger whose outlet fluid parameters are determined by the following energy balance equations. The model assumes no conduction within and between tubes, and uniform air temperature and velocity entering to the gas cooler.

For a given segment j, the energy balance equation can be expressed as follows:

Air side:

$$Q_j = m_{aj} Cp_a \ (T_{ae,j} - T_{ai}) \tag{1}$$

Refrigerant side:

$$Q_j = m_r \left\{ h(T,P)_j - h(T,P)_{j-1} \right\} \tag{2}$$

Heat transfer between air and surface:

$$Q_j = h_a \eta_a A_{a,j} \left[(T_{ae,j} - T_{ai}) \Big/ \ln\left(\frac{T_{s,j} - T_{ae,j}}{T_{s,j} - T_{ai}} \right) \right] \tag{3}$$

Heat transfer between surface and refrigerant:

$$Q_j = h_{r,j} \eta_{r,j} A_{r,j} \left[(T_{r,j-1} - T_{r,j}) / \ln\left(\frac{T_{r,j-1} - T_{s,j}}{T_{r,j} - T_{s,j}} \right) \right] \tag{4}$$

For the supercritical R744, the heat transfer coefficient is calculated by using the Gnielinski (1976) correlation:

$$Nu_D = \frac{(f/8)(\mathrm{Re}_D - 1000)\,\mathrm{Pr}}{1 + 12.7(f/8)^{1/2}(\mathrm{Pr}^{2/3} - 1)} \quad 0.5 < \mathrm{Pr} < 2000;\ 2300 < \mathrm{Re_D} < 5 \times 10^5 \tag{5}$$

which was found by Rieberer (1999) to be the best for single-phase R744 at supercritical and subcritical conditions after comparing six correlations for smooth tube with 7.8mm inner diameter. The correlations differed by less than 30% over a wide temperature range. The difference between calculation from Gnielinski's correlation and Rieberer's measurement was negligible at mass flux (~500kg/m^{2}s) and heat fluxes (~40kW/m^2) typical of CO2 gas coolers. The friction factor was calculated from Churchill (1977) correlation:

$$f = 8\left\{ \left(\frac{8}{\mathrm{Re}}\right)^{12} + \left[\left(2.457 \ln\left(\frac{1}{\left(\frac{7}{\mathrm{Re}}\right)^{0.9} + 0.27\delta} \right)\right)^{16} + \left(\frac{37530}{\mathrm{Re}}\right)^{16} \right]^{-3/2} \right\}^{1/12} \tag{6}$$

which spans all flow regimes and all relative roughness (δ). The absolute roughness for extruded aluminum microchannel tubing is about 4.2μm to 5.3μm based on our actual measurement, which is very close to the "typical" number of 5μm (Memory, 1999), and this number will be used in the pressure drop calculation.

The air-side heat transfer correlation selected for the model was proposed by Chang and Wang (1997). It was selected because it covered the widest array of geometry's and is one of the most recently published louvered fin airside heat transfer coefficient correlations.

The Chang and Wang correlation was defined in terms of the dimensionless heat transfer coefficient, the Colburn j-factor:

$$j = \mathrm{Re}_{Lp}^{-0.49}\left(\frac{\theta}{90}\right)^{0.27}\left(\frac{Fp}{Lp}\right)^{-0.14}\left(\frac{Fl}{Lp}\right)^{-0.29}\left(\frac{Td}{Lp}\right)^{-0.23}\left(\frac{Ll}{Lp}\right)^{0.68}\left(\frac{Tp}{Lp}\right)^{-0.28}\left(\frac{\delta_f}{Lp}\right)^{-0.05} \quad (7)$$

The above correlation can be used in the Reynolds number range from 100 to 3000 based on the louver pitch. The Reynolds number of our experimental data is from 160 to 250.

The surface efficiency is simply an area-weighted fin efficiency defined by:

$$\eta_a = 1 - \frac{A_f}{A_a}(1 - \eta_f) \quad (8)$$

The fin efficiency of longitudinal fin is:

$$\eta_f = \frac{\tanh(mL)}{mL} \qquad \text{where} \qquad mL = \sqrt{2\frac{h_a}{k_f \delta_f}}\frac{Fl}{2}$$

For our range of test conditions, the fin efficiency ranged between 0.89 to 0.91. The surface efficiency for the refrigerant side was set equal to 1 because the circular ports were unfinned. Resistance due to conduction through the tube material is assumed to be negligible.

The total refrigerant side pressure drop across the heat exchanger can be calculated by add the pressure drop of each pass together. These pressure drops include friction and acceleration (deceleration) in the tubes, local pressure drops in the elbows and headers.

For inlet and exit tubes, the pressure drop can be calculated from:

$$\Delta P = f\frac{L}{D}\frac{G^2}{2\rho} \quad (9)$$

The friction factor f was calculated from Eq. 6. The inlet tube length (from transducer to inlet elbow) and exit tube length were about 1.62m and 0.12m, respectively, and their inner diameters were 6.3mm.

The local pressure drop for this 90° sharp elbow with constant cross-sectional area can be calculated from local pressure loss equation

$$\Delta P = \zeta\frac{G^2}{2\rho} \quad (10)$$

Where $\zeta = 1.2$ is the local pressure drop coefficient (Idelchik 1994). There are three 90° sharp elbows in the inlet tube part and one in the exit tube part.

The local pressure drops for heat exchanger inlet/exit elbows with sudden cross-section area changes can be expressed as:

$$\Delta P_{ie} = \frac{G_{in}^2}{2\rho}(\zeta_{inlet} - 1 + \sigma^2)$$
$$\Delta P_{ee} = \frac{G_{out}^2}{2\rho}(\zeta_{exitt} + 1 - \sigma^2) \qquad (11)$$

From the handbook (Idelchik, 1994), for similar elbows when Reynolds number is greater than $2x10^5$, the coefficient for inlet elbow (ζ_{inlet}) is about 0.82, for exit elbow (ζ_{exit}) is about 0.45.

The pressure drops in the inlet and exit header tube due to free flow area changes and friction, can be calculated from

$$\Delta P = \sum_{i=1}^{N}(f_{ihd,i}\frac{\Delta L_{hd}}{D_{ihd}} + k_{loss,ihd})\frac{G_{ihd,i}^2}{2\rho_{ihd,i}} + \sum_{i=N+1}^{N1}(f_{ehd,i}\frac{\Delta L_{hd}}{D_{ehd}} + k_{loss,ehd})\frac{G_{ehd,i}^2}{2\rho_{ehd,i}} \qquad (12)$$

There is no local pressure drop coefficient for our unique shape of header tube, so a nitrogen test was conducted with a similar single-pass heat exchanger with identical headers, and the coefficients were determined to be about $k_{loss,ihd}$ 0.25 for inlet header, and $k_{loss,ihd}$ 0.68 for exit header (Yin et al., 2000a).

The pressure drop for port inlet/exit part of each microchannel tube (tube N) can be treated as a sudden contraction and expansion, and it can be calculated from

$$\Delta P = \frac{G_{port,N}^2}{2\rho_{in,N}}(1 + \xi_{cont} - \sigma^2) + \frac{G_{ehd,N}^2}{2\rho_{out,N}}(\xi_{expan} - 1 + \sigma^2) \qquad (13)$$

Because it is difficult to define precisely the area ratio for this particular header/tube configuration, the inlet contraction (ξ_{cont}) and exit expansion (ξ_{expan}) coefficients were taken from Idelchik's handbook for the maximum area ratio (10:1). For the range of flow rates of the experimental data, the values for the two coefficients are 0.45 and 0.81, respectively.

Because the model uses finite element method, the in-tube pressure drop for each port was also calculated the 10 segments of each tube, accounting for friction and acceleration (deceleration).

$$\Delta P = G_{port,N}^2\left[\sum_{i=1}^{10}(\frac{\Delta L_{tube}}{D_{port}}\frac{f_{tube,N,i}}{(\rho_{ig,N} + \rho_{i-1,N})} + (\frac{1}{\rho_{i,N}} - \frac{1}{\rho_{i-1,N}})\right] \qquad (14)$$

In order to simplify this part of the data analysis, uniform mass flow rate distribution was assumed for each port and tube, and the pressure drop calculation followed the central tube in each pass. The total pressure drop of each pass is the sum of the pressure drop in the inlet header tube (half length), sudden contraction to middle tube, friction along this tube, exit expansion from this tube and along the rest half length of the exit header tube.

The air side pressure drop was calculated by using the method described by Kays and London (1998) using the Chang and Wang (1996) friction factor correlation.

$$f = 0.805\,\mathrm{Re}_{Lp}^{-0.514}\left(\frac{Fp}{Lp}\right)^{-0.72}\left(\frac{Fl}{Lp}\right)^{-1.22}\left(\frac{Ll}{Lp}\right)^{1.97} \tag{15}$$

The given conditions for each segment are: air inlet temperature, airflow rate, refrigerant flow rate and refrigerant inlet pressure and temperature. There are four unknowns in equations 1 to 4, so the problem can be solved simultaneously for refrigerant exit pressure and temperature, gas cooler capacity and air exit temperature.

The whole model was solved by using EES (Klein and Alvarado, 1995) and its thermophysical property data, except for the properties of R744 which were obtained from the extended BWR equation of state (National Institute of Standards and Technology REFPROP, 1998) because it was known to be more accurate in the supercritical region than the equation used in the EES.

Model verification

Figures 4 to 6 compare the model predictions with the measured data. As shown on Figure 4 and 5, for most of the experimental data, the model predicts the capacity within ±2% and exit refrigerant temperature within ±0.7°C, which is within the experimental error (±2% and 1°C). Figure 5 shows that the model systematically underpredicted the refrigerant pressure drop by about a factor of three, except a few very low flow rates. Since the pressure drop was measured by using two absolute pressure tranducers and each has an uncertainty of ±52kPa (range: 20.7MPa, accuracy: ±0.25% FS), the pressure drop measurements lower than about 70kPa lie within the measurement error.

This model was based on the log mean temperature method, as shown in Equation 3 and 4, because the ε-NTU method (crossflow with both fluids unmixed) is accurate only for the case where the heat capacity ratio is unity (Incropera and Dewitt, 1996). In the third pass of the gas cooler, the heat capacity ratio is very small (about 0.01 to 0.2) when the fluid is near the critical point.

Figure 6 presents the experimental and calculated refrigerant side pressure drop. The reason for the serious underprediction (at high pressure drop range) of pressure drop cannot be known with certainty. However considerable insight can be gained from a large number of nitrogen flow tests conducted on a similar heat exchanger manufactured at the same time from the same batch of tubes and identical headers (Yin et al., 2000a).

For a similar heat exchanger subjected to extensive nitrogen flow testing, Yin et al (2000a). found the average port diameter to be 94% of nominal and that 39% of ports were blocked. These estimates were confirmed by cutting the heat exchanger, measuring port diameters and counting the number of ports blocked by brazing flux. Assuming that the same dimensional changes occurred during fabrication of this particular gas cooler, the simulations were repeated using the new dimensions. Figure 7 shows the result. After adjusting for manufacturing defects, the model could predict the refrigerant side pressure drop with good agreement.

Since in-tube pressure drop is so sensitive to diameter and mass flux, uncertainties about the manufacturing process may limit the accuracy of heat exchanger simulation models, especially in the case of those having sub-millimeter port diameters. Fortunately the effect of pressure drop on gas cooler capacity is rather small. Moreover, the accuracy of the model presented here suggests that port diameter and the number of blocked ports could be estimated (using least squares parameter estimation techniques) from nitrogen flow tests data obtained at only a few typical Reynolds numbers, and used to predict the performance at other conditions.

Table 3 shows the distribution of the pressure drops for a given condition with mass flow rate of 54.8 g/s. All the pressure drops are in kPa. The inlet tube and elbow part includes a 6.3mm diameter copper tube 1.62m long, three 90° elbows and the heat exchanger inlet elbow. The exit tube length is about 0.12m and with one additional 90° elbows. As shown in this table, the predicted total pressure drop is about 407kPa, which is about 2% higher than the measured value. About 75% of the pressure drop is due to the friction along the tube ports. The port contraction and expansion account for about 5% of the total pressure drop.

For air side pressure drop, the model can predict the data within 10 Pa for the three different air flow rates.

Application of the model

One of the many advantages of model is that it facilitates analysis of details of the thermodynamic process. Figure 8 shows the temperature and specific heat distribution of R744 along the flow length of the gas cooler for the operating condition corresponding to the last row of Table 2. For different operating conditions, the shape of the specific heat curve may be different. With temperature and pressure close to critical, the specific heat value increases. Comparing the air temperature at gas cooler inlet and refrigerant temperature (Tr) in Figure 8, shows that the temperature difference between air and refrigerant in the second and third passes are much smaller than in the first pass. Figure 9 shows how the heat transfer coefficient varies substantially along the flow length, due mainly to the CO2 property changes rather than changes in Reynolds number.

In the transtical refrigeration cycle, the enthalpy at gas cooler exit is most important because it translates directly into an increase in system capacity. In an ideal gas cooler, the refrigerant exit temperature is equal to the air inlet temperature and the refrigerant side pressure drop is zero. Figure 10 shows how refrigerant enthalpy changes along the flow length. The ideal exit condition was also shown on the Figure. It is clear that the prototype gas cooler is far from ideal.

By increasing the number of passes, better heat transfer performance may be expected due to higher refrigerant side heat transfer, but at the expense of increasing pressure drop. In order to compare the different circuiting arrangements, the model was used to predict the performance of the prototype, plus four hypothetical designs having different numbers of passes as shown in Table 4. Figure 11 shows the exit enthalpy from gas cooler and pressure drop in the refrigerant side. The results suggest that 3-pass gas cooler may be the best, but the difference between three and five passes is very small. At the higher mass flow rates, the 4- and 5-pass heat exchangers will experience much higher pressure drops.

Another way to improve the gas cooler performance is to use multiple slabs instead of multiple passes. If using more slabs, the heat transfer process will be closer to an ideal counter flow heat exchanger. Table 5 shows the simulation result for a three-slab gas cooler having the same dimensions (height, width and depth), fin height, and fin density as the 3-pass prototype tested. As shown in the table, the performance of multiple slab gas cooler is much better than multiple-pass design. The approach temperature difference was reduced from 6.8°C to 4.3°C, ΔP was reduced by a factor of 5.6. The enthalpy at the gas cooler exit was reduced, so the capacity was increased by (303-287)x 0.0229, that is 0.3kW. This idea is described in Yin et al. (2000b).

Conclusions

A finite element model for supercritical cross-flow gas cooler was developed, to model accurately the variations in thermodynamic and transport properties near the critical point. It was verified by data obtained in more than 350 experiments. The model can predict R744 exit temperature from gas cooler within ±0.7°C for most of the experimental data, given only the inlet conditions. Different arrangements of the gas cooler within the original package dimensions were simulated and it was found that the 3-pass gas cooler is the best the single-slab designs. However using multiple slabs is the more effective way to improve the performance.

Acknowledgement

We are grateful to Hydro Aluminum A. S. for supporting this research over a 3 year period.

Nomenclature

A	area [m^2]
Cp	specific heat [kJ/kg.K]
D	hydraulic diameter [m]
Dp	pressure drop [kPa]
f	friction factor
Fl	fin length [mm]
Fd	fin depth [mm]
Fp	fin pitch [mm]
G	mass velocity [$kg/m^2.s$]
h	heat transfer coefficient [$W/m^2.°C$]
h	specific enthalpy [kJ/kg]
j	Colburn factor
k	thermal conductivity [$W/m^2.°C$]
Ll	louver length [mm]
Lp	louver pitch [mm]
m	mass flow rate [kg/s or g/s]
Nu	Nusselt number

P	pressure [kPa]
Pr	Prandtl number
P_r	Pressure ratio
Re	Reynolds number
T	temperature [°C]
Td	tube depth [mm]
Tp	tube pitch [mm]

Greek Letters

ρ	density [kg/m^3]
η	efficiency
δ	thickness of fin [mm]
θ	louver angle [deg]
ζ	local pressure drop coefficient
σ	area ratio

Subscripts:

a	air
r	refrigerant
i	inlet
id	ideal case
ihd	inlet header
j	segment
e	exit
ehd	exit header
f	fin
s	surface

References

Boewe, D., Park, Y.C., Yin, J., Bullard, C.W., Hrnjak, P.S., The Role of a Suction Line Heat Exchanger in Transcritical R744 Mobile A/C Systems. SAE International Congress and Exposition, Paper 1999-01-0583, 1999a.

Boewe, D., Hrnjak, P., Evaluation of an R744 mobile air conditioning system. ACRC Contract Report, ACRC CR-17, University of Illinois, 1999b.

Chang, Y. J. and Wang, C. C., Air Side Performance of Brazed Aluminum Heat Exchangers. *Journal of Enhanced Heat Transfer*, 1996, **3**(1), 15-28.

Chang, Y. J. and Wang, C. C., A Generalized Heat Transfer Correlation for Louver Fin Geometry. *Int. J. Heat Mass Transfer*, 1997, **40**(3), 533-544

Churchill, S. W., Friction-factor Equation Spans All Fluid Flow Regimes. *Chemical Engineering*, 1977, No. 7, 91-92.

Gnielinski, V., New Equations for Heat and Mass Transfer in Turbulent Pipe and Channel Flow. *Int. Chem. Eng.*, 1976, Vol. 16, 359-368.

Idelchik, I. E., *Handbook of Hydraulic Resistance.* 3rd Edition, CRC Press (1994).

Incropera, F. P. and Dewitt, D. P., *Fundamentals of Heat and Mass Transfer.* John Wiley & Sons, 4th Edition (1996).

Kays W.M. and London A. L., *Compact Heat Exchangers.* third edition. Krieger Publishing Company (1998).

Klein, S. and Alvarado, F. *Engineering Equation Solver.* F-Chart Software, Middleton, WI (1995).

Lorentzen, G., Pettersen, J., A New, Efficient and Environmentally Benign System for Car Air-Conditioning. *Int. Journal of Refrigeration*, 1993, **16**(1), 4-12.

McEnaney, R.P., Boewe, D.E., Yin, J.M., Park, Y.C., Bullard, C.W., Hrnjak, P.S., Experimental Comparison of Mobile A/C Systems when Operated With Transcritical CO_2 Versus Conventional R134a. International Refrigeration Conference at Purdue, 1998, 145-150.

Pettersen, J. and Skaugen G., Operation of Trans-Critical CoO2 Vapour Compression Circuits in Vehicle Air Conditioning. International Institute of Refrigeration, Commission B2, Hannover, Germany, 10-13 May, 495-509, 1994.

McEnaney, R.P., Park, Y.C., Yin, J.M., Hrnjak, P.S., Performance of the Prototype of Transcritical R744

Mobile A/C System. SAE International Congress and Exposition, Paper 1999-01-0872, 1999.

Memory, S. B., Private communication (1999).

REFPROP Version 6.0, NIST Thermodynamic and Transport Properties of Refrigerants and Refrigerant Mixtures. U.S. Department of Commerce, Gaithersburg, Maryland, 1998.

Rieberer, R., CO2 Properties. IIR Workshop on CO2 Technology in Refrigeration, Heat Pump and Air Conditioning Systems, Mainz, Germany, 1999.

Robinson, D. M. and Groll E. A., Efficiencies of transcritical CO2 cycles with and without an expansion turbine. *Int. J. Refrig.* 1998, **21**(7), 577-589.

Yin, J. M., Bullard, C. W. and Hrnjak, P. S., Pressure drop measurements in microchannel heat exchanger. University of Illinois at Urbana-Champaign, CR-40, 2000a

Yin, J. M., Bullard, C. W. and Hrnjak, P. S., Design Strategies For R744 Gas Coolers. International Refrigeration Conference at Purdue, 2000b.

Table 1. Dimensions and characteristics of the gas cooler used for experimental validation of the model.

Gas Cooler Characteristics	
Mass (kg)	2.3
Face Area (cm^2)	1950
Core Depth (cm)	1.65
Core Volume (cm^3)	3320
Airside Area (m^2)	5.2
Refrigerant Side Area (m^2)	0.49
Fin Density (fins/in)	22
Louver Angle (^{o})	23
Tube Length (mm)	545
Number of Ports	11
Port Diameter (mm)	0.79
Web Thickness (mm)	0.70
Wall Thickness (mm)	0.43
Fin Height (mm)	8.89
Fin Thickness (mm)	0.10
Louver Height (mm)	7.16
Louver Pitch (mm)	0.99
Number of Louvers	2 x 6
Louver redirection Length (mm)	1.7
Louver entry Length (mm)	1.7
Header tube diameter (mm)	2@7
Inlet/exit elbow tube diameter (mm)	7

Table 2 Gas cooler performance data

m_r [g/s]	P_{ri} [kPa]	DP_r [kPa]	T_{ri} [°C]	T_{re} [°C]	m_a [g/s]	T_{ai} [°C]	DP_a [Pa]
34.74	11007	137.7	108.9	48.2	542	43.0	43
56.36	10792	421.6	138.6	50.2	701	43.5	61
39.98	12014	155.4	125.4	49.0	699	44.3	62
26.39	12464	62.7	115.8	58.0	457	55.1	45
37.84	10937	116.3	124.7	49.0	537	42.7	46
22.37	9556	60.9	97.9	45.8	453	43.1	39
27.12	10982	97.5	101.2	56.0	459	53.9	46
27.48	9333	99.0	91.0	45.5	452	43.0	39
31.49	8858	103.6	66.5	38.4	452	31.8	34
24.07	14390	25.4	113.3	45.4	452	43.0	40
22.08	10555	28.2	103.0	35.9	453	32.4	34
22.06	11392	37.2	114.8	46.8	437	43.4	38
25.17	8386	91.1	87.4	36.8	451	31.5	32
38.49	10278	197.9	118.9	48.4	537	43.3	47
19.6	12460	27.6	126.6	46.0	454	43.5	40
44.31	9061	337.3	104.0	46.4	541	43.4	47
21.67	9514	24.0	102.0	36.9	451	32.4	34
23.56	9841	52.7	107.1	46.0	452	42.8	39
45.58	8587	344.3	101.7	45.0	536	42.7	46
24.68	8460	67.3	89.0	37.2	451	31.8	33
47.53	8677	389.9	97.8	45.1	535	42.7	46
25.92	9387	92.2	97.0	45.7	455	43.1	40
26.6	8435	78.0	81.3	37.2	453	32.2	34
25.98	10014	84.4	96.6	46.5	461	42.9	40
42.73	9713	239.4	108.0	47.5	539	43.2	48
25.25	8328	66.2	84.4	36.8	453	32.4	34
25.11	9593	78.5	96.9	45.7	453	43.0	41
43.12	9200	286.9	105.4	46.3	539	42.9	47
26	8331	59.1	81.2	36.9	453	32.1	35
37.69	10259	166.0	120.9	48.6	540	43.7	49
22.83	9537	18.9	93.8	37.4	450	32.1	34
26.04	7659	73.8	78.2	32.5	454	26.8	32
25.45	8359	66.1	87.3	36.7	456	31.7	35
32.63	9242	145.0	83.3	45.5	455	43.3	38
26.06	9349	93.2	94.1	45.2	536	43.8	47
25.55	9385	85.3	95.4	44.9	710	43.6	66
24.72	7826	57.1	79.9	33.4	448	26.8	31
26.23	8204	81.9	82.3	36.4	449	32.4	34
20.78	9833	46.2	106.8	46.0	451	43.6	40
34.86	10735	168.9	129.8	48.7	540	43.7	48
32.91	9879	150.5	110.5	47.3	502	43.7	44
31.47	10315	127.9	116.0	48.3	501	44.1	45

m_r [g/s]	P_{ri} [kPa]	DP_r [kPa]	T_{ri} [°C]	T_{re} [°C]	m_a [g/s]	T_{ai} [°C]	DP_a [Pa]
29.95	10772	109.4	121.1	48.2	502	43.7	45
28.82	11251	92.8	125.8	48.1	501	43.6	45
27.94	11745	84.0	130.3	48.0	501	43.7	45
23.02	8303	29.6	83.3	33.1	455	26.7	29
22.90	8413	31.0	85.5	33.7	447	27.0	31

Table 3 Pressure drop along flow path [kPa]

Measured	Inlet tube and elbow	Inlet header	Contraction	Friction	Expansion	Exit header	Exit tube and elbow
399	66	2	7	305	11	5	9

Table 4 Model prediction results for multiple pass gas coolers

Number of passes	Tube/pass	T_{re}	h_{re}	DP	T_{ai}	h_{ideal}
1	34	35.9	325	4	27	269
2	17/17	34.4	307	20		
3	13/11/10	33.8	303	56		
4	10/9/8/7	33.4	301	121		
5	8/7/7/6/6	33.2	302	228		

Table 5 Performance of three slab gas cooler

h_i (kJ/kg)	h_e (kJ/kg)	h_{ideal} (kJ/kg)	T_e (°C)	T_{ideal} (°C)	DP (kPa)
498	287	269	31.3	27	10

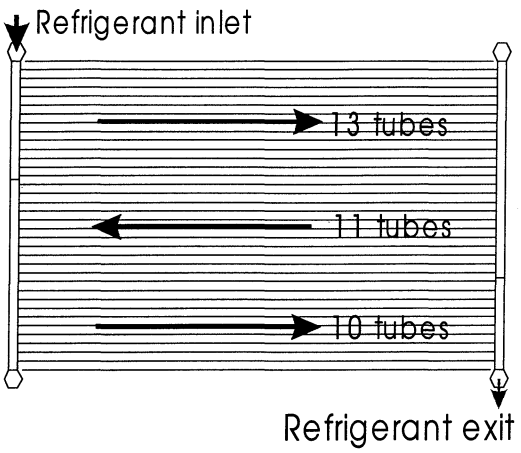

Figure 1 Schematic of CO2 gas cooler

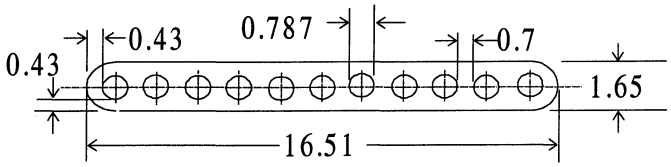

Figure 2 Cross-section of microchannel tube [mm]

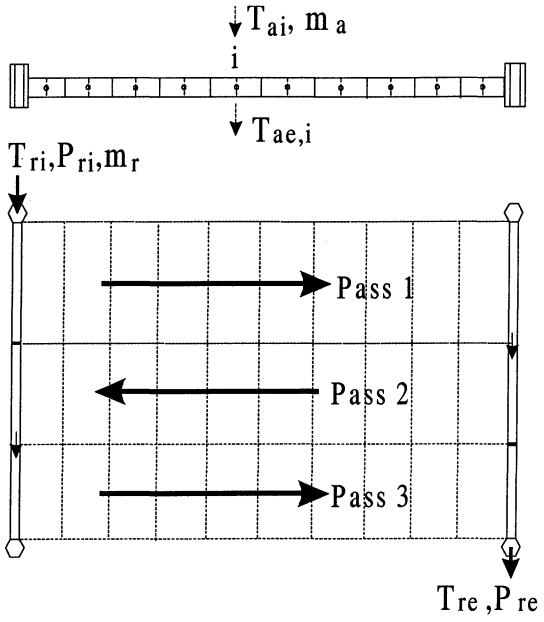

Figure 3 CO2 gas cooler

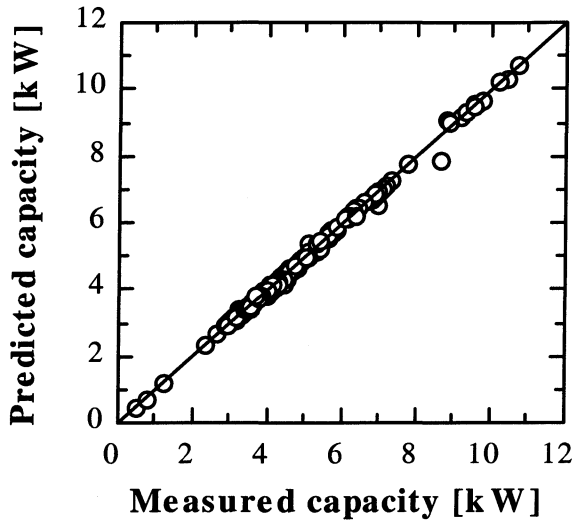

Figure 4. Experimental vs model predicted capacity

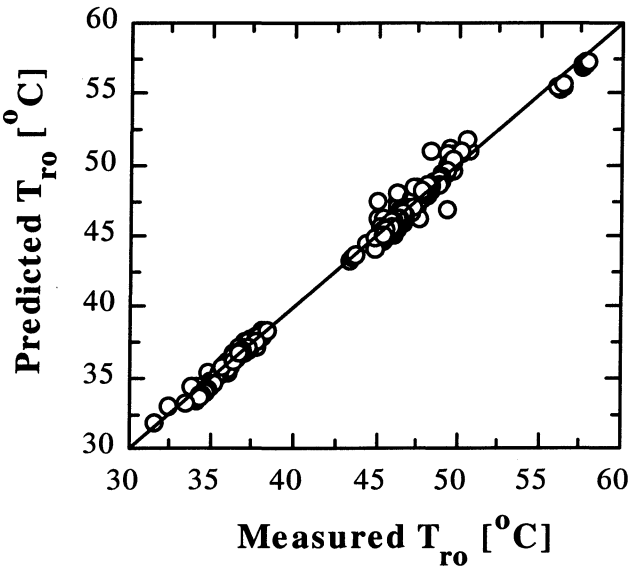

Figure 5. Refrigerant exit temperatures

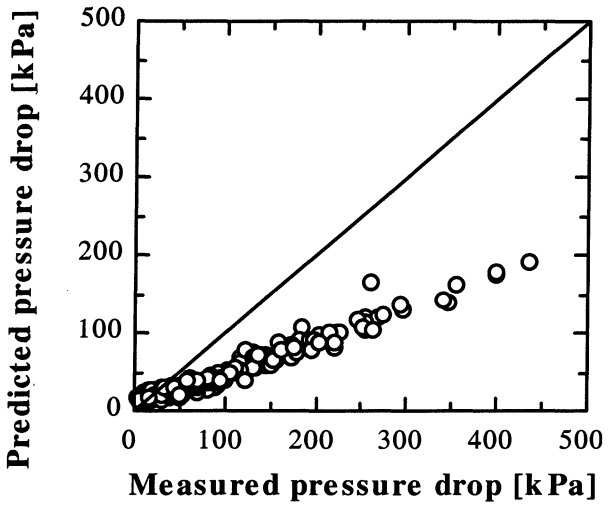

Figure 6. Accuracy of pressure drop calculation (no manufacturing defects)

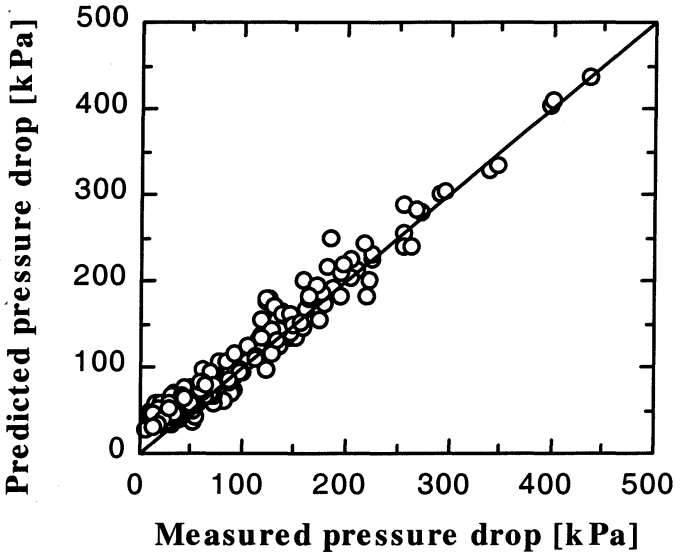

Figure 7. Refrigerant pressure drop (accounting for observed manufacturing defects)

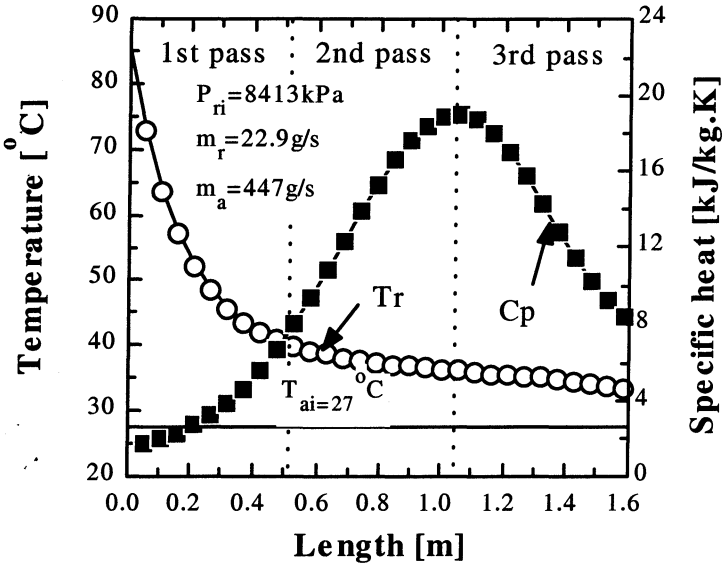

Figure 8. Temperature and specific heat along gas cooler flow length

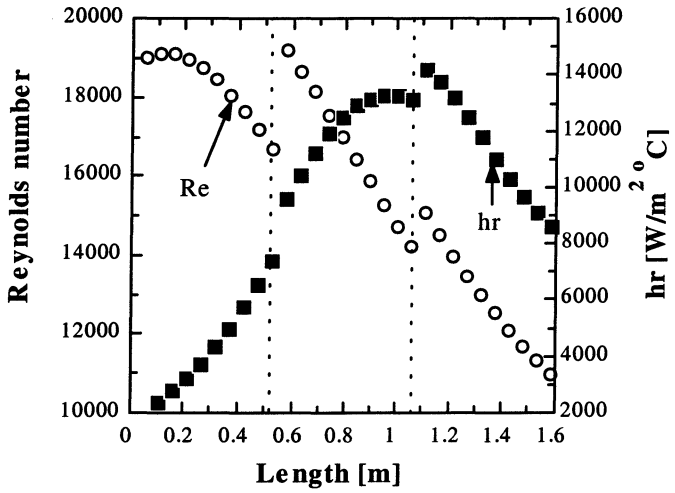

Figure 9. Reynolds number and heat transfer coefficient along gas cooler flow length

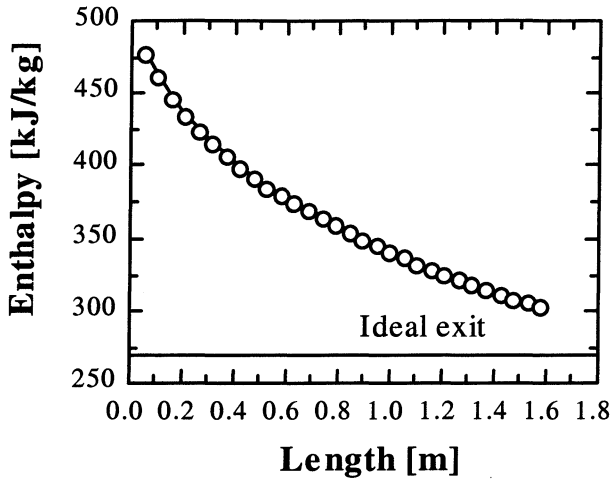

Figure 10. Refrigerant enthalpy along heat exchanger flow length

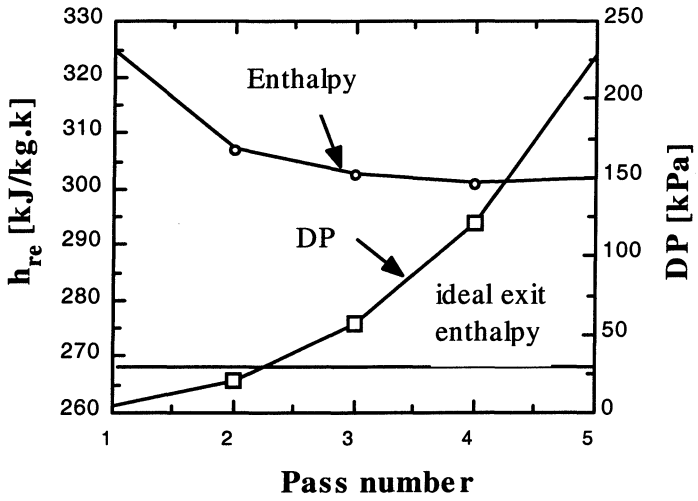

Figure 11. Effect of increasing number of passes